Self-*Q*-switching with interferometers

Gang Wang,[1,*] Chenxi Zhang,[1,*] Hong Jin,[1] Lijun Xu,[1] and Bo Fu[1,2,†]
[1]*School of Instrumentation and Optoelectronic Engineering, Beihang University, Beijing 100191, China*
[2]*Key Laboratory of Big Data-Based Precision Medicine Ministry of Industry and Information Technology, School of Engineering Medicine, Beihang University, Beijing 100191, China*

(Received 18 September 2023; accepted 14 February 2024; published 6 March 2024)

Self-*Q*-switching facilitates the generation of pulsed lasers without resorting to conventional *Q*-switched techniques, while there has been limited research and theoretical development in this area. In this paper, we introduce an interference-based self-*Q*-switching phenomenon and conduct a comprehensive numerical analysis. Our findings reveal distinct properties when compared to traditional *Q*-switching, underscoring the role of interferometers. Through a combination of experimental measurements and waveguide simulations, we propose a self-*Q*-switching mechanism based on jitter-induced filtering. This mechanism aligns well with our experimental observations and provides an explanation from the perspective of the frequency domain. This research contributes to the understanding of self-*Q*-switching theory and its excitation.

DOI: 10.1103/PhysRevA.109.033507

I. INTRODUCTION

The quality factor Q of a laser resonator is used to quantify its quality, defined as $2\pi^*$ (energy stored in the resonator/energy lost per cycle) [1]. By varying the quality factor within a laser cavity, it is possible to instantaneously release the stored energy within the active medium, resulting in *Q*-switched pulses with peak powers several orders of magnitude higher than continuous-wave lasers [2]. *Q*-switched pulses find applications in modern technology, such as laser therapy [3,4], sensing [5], and laser-induced breakdown spectroscopy [6]. Depending on the need for external input signals, *Q*-switching techniques can be categorized as active or passive [7]. Active *Q*-switching requires external components such as acousto-optic modulators [8] or electro-optic modulators [9] to change the quality factor, while passive *Q*-switching, though not requiring complex external input devices, necessitates the preparation of specific saturable absorbers [10].

Self-*Q*-switching (SQS) is an intriguing phenomenon observed in laser resonators, where *Q*-switching occurs spontaneously without the need for a dedicated saturable absorber [11–23]. However, the underlying principles of SQS have been relatively understudied, with multiple hypotheses proposed, primarily relying on time-domain explanations involving gain properties. Some suggest it is due to particle interactions within energy levels [19,24], some attribute it to thermal-induced lensing [13,17,25], and others propose that unsaturated gain regions within the fiber contribute to saturable absorption [11,12,17]. While exploring answers within gain fibers seems intuitive and plausible, a curious observation in SQS reports involves the presence of interferometers [11,17], which has also been substantiated as critical in our experiment. This raises questions about the role of interferometers in SQS phenomena.

In this paper, we introduce and validate an interferometer-based mechanism for achieving SQS. We report SQS phenomena through experiments, analyze the characteristics to deduce the underlying principles, and validate them theoretically through simulations. Initially, we achieve SQS in an erbium-doped fiber laser and demonstrate that SQS cannot be realized in the absence of an interferometer, highlighting the crucial role of interferometers in SQS. Subsequently, we measure and simulate the behavior of the interferometer, capturing variations in the temporal and spectral output concerning the wavelength and optical path difference. We further simulate SQS based on our experimental and simulation results, suggesting that the filtering effect in the interferometer triggers the laser to enter a steady *Q*-switching state. Our report experimentally characterizes the complexity of SQS pulses and theoretically proves the mechanism behind laser self-*Q*-switching from the perspective of the frequency domain.

II. RESULTS

A. Generation of self-*Q*-switched pulses

Figure 1(a) illustrates the laser setup, where a wavelength division multiplexer (WDM) couples a 980-nm pump into the cavity, an 0.5-m erbium-doped fiber (EDF) generates a 1550 nm signal, a polarization-independent isolator (PIISO) ensures unidirectional laser operation, and a polarization controller (PC) fine-tunes the polarization state. Two 50 : 50 optical couplers (OCs) form a Mach-Zehnder interferometer (MZI) within the cavity. The total cavity length is 13 m. Notably, there are no polarization-related components inside the cavity. We initially suspected whether the MZI acted similar to a nonlinear optical loop mirror [26], but the nonlinear

*These authors contributed equally to this work.
†fubo10@buaa.edu.cn

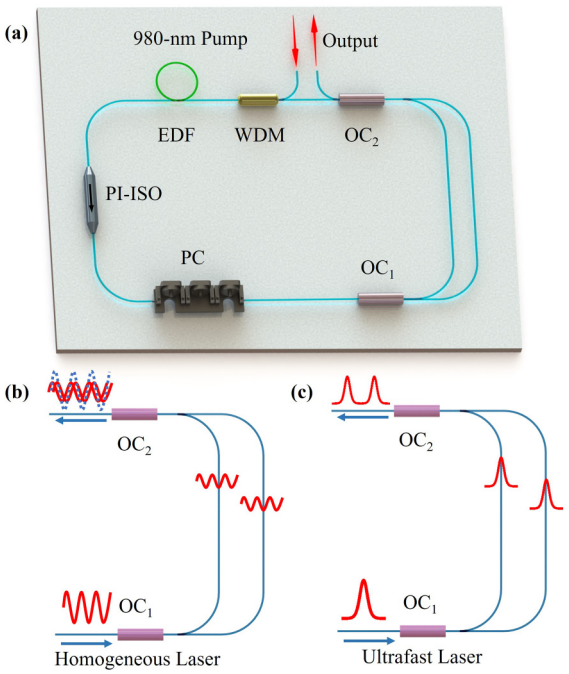

FIG. 1. Experimental setup of the SQS laser and the modulation of MZI on different input lasers. (a) Schematic of the laser setup, with no polarization-dependent components nor saturable absorbers inside the cavity. Apart from the two OCs forming the MZI, all other components are fundamental elements for a generating 1.5-μm unidirectional laser. (b) Spectral modulation of MZI on an input monochromatic continuous wave, resulting in losses corresponding to the optical path difference, with a portion of the loss exiting the cavity through the OC. (c) Temporal modulation of MZI on an input ultrashort pulse. The initial pulse is split into two, and upon recombination a bound-state-like structure emerges due to the optical path difference.

phase shift induced by low-input intensity is insufficient to induce artificial saturable absorption in the MZI. Figures 1(b) and 1(c) demonstrate the modulation effects of MZI on different input light. When the homogeneous laser is input, it is split into two paths, which recombine after experiencing different optical paths, resulting in an output intensity that varies with the optical path difference. In the case of ultrafast laser input, the pulses converge after traversing different optical paths, forming a bound-state-like structure [27,28]. Specifically, the dual-pulse output resembles a two-soliton bound state, representing closely spaced short-pulse interference with a pulse interval matching the optical path difference of the MZI.

Self-Q-switched pulses are achieved in the laser cavity as shown in Fig. 2. Figures 2(a)–2(c) present the temporal waveform and spectrum of SQS pulses. Once the pump power exceeds 50 mW, 1550-nm laser emission initiates as shown in Fig. 2(d). Importantly, in our laser cavity, the Q-switching threshold closely matches the continuous-wave lasing threshold, meaning that Q-switching occurs almost immediately after the onset of continuous-wave lasing. This distinguishes it from conventional Q-switched lasers [29,30], confirming the extremely low saturable absorption threshold within the cavity. As the pump power continues to increase, the output power exhibits linear growth. Figures 2(e) and 2(f) demonstrate changes in the pulse properties as the pump power increases, which exhibit typical Q-switched characteristics. Figures 2(g) and 2(h) show single- and double-peak spectra under different polarization states, allowing for multiwavelength operation.

The SQS phenomenon we observe exhibits unique characteristics that facilitate the exploration of its mechanism. First, SQS disappears when the MZI is removed, an observation unexplainable by existing SQS theories, showing the dependence of interferometers for SQS generation. Second, Q-switching occurs as soon as lasing initiates, indicating an exceptionally low Q-switching threshold, differing significantly from passive Q-switching that is typically with a distinct threshold compared to continuous-wave lasing. Additionally, Q-switching outputs can be achieved under extensive polarization angles, which suggests that Q-switching is independent of a specific polarization state, eliminating the possibility of nonlinear polarization rotation [31] causing Q-switching. Furthermore, Q-switching rapidly disappears at high pump powers, which indicates that incompletely pumped EDF contributes to the generation of SQS. Indeed, saturable absorption exists in unpumped gain fibers [32], which exhibit a lower saturation intensity and a larger modulation depth compared to typical real saturable absorbers [33–35]. Lastly, the central wavelength of Q-switching is tunable and the spectra are sensitive to polarization states.

B. Measurement of the interferometer

As the influence of the MZI depends on the optical path difference, changes in the optical path difference can be observed by inputting external mode-locked pulses to create a bound-state-like structure. Figures 3(a) and 3(b) show the pulse train and spectrum of the mode-locked signal. The spectrum of the complete external input signal is shown in Fig. 3(c), including both continuous-wave and mode-locked components. When this signal is input into the MZI, interference of the continuous wave results in overall fluctuations as shown in Fig. 3(d). The mode-locked component experiences signal superposition, creating features resembling two-soliton bound states [27] in the spectrum and demonstrating the phase difference after passing through the two arms, as shown in Figs. 3(e)–3(h). The phase variations reflect changes in the optical path difference, resulting in energy fluctuations in the continuous wave. The optical path difference is approximately 0.93 mm calculated from a pulse interval $\Delta t = 1/\Delta\upsilon = 3.1$ ps, where $\Delta\upsilon$ is the modulation period of the frequency spectrum.

The filtering effect caused by the MZI interference continues to affect SQS generation and output. Therefore, we conducted a simulation based on the measured optical path difference to study the filtering effect of the MZI as a function of input wavelength and optical path difference. Figures 4(a) and 4(b) illustrate the schematic and electric field distribution of the MZI. Figure 4(c) depicts the transmission rate as a function of input wavelength and optical path difference. The profiles are split by solid and dashed lines, and the cross-sectional profiles are represented in Fig. 4(d). It is observed that the phase difference between the two output ports remains at π, and the center of filter curve shifts with changes

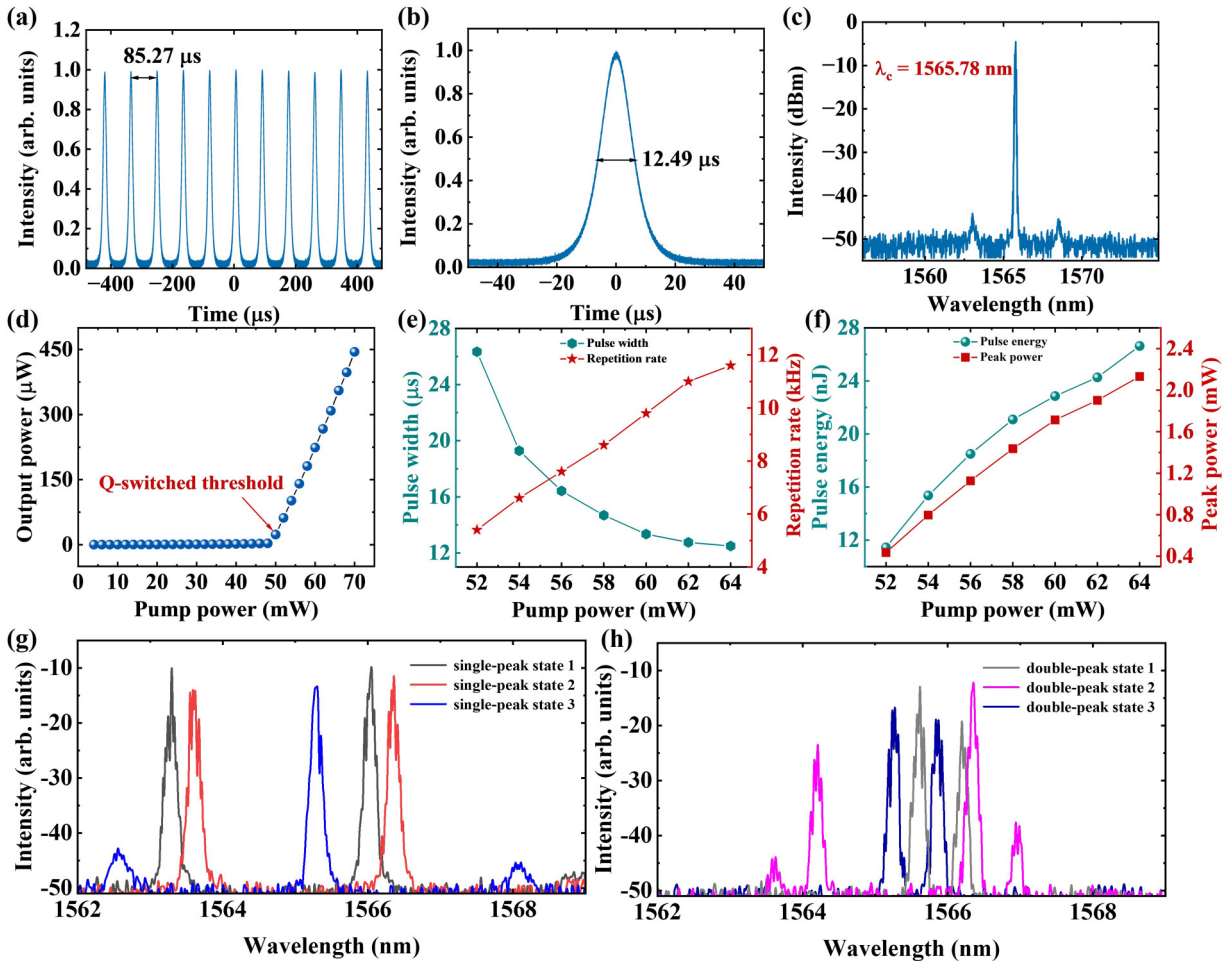

FIG. 2. Experimental measurements of the SQS laser. (a) Oscilloscope trace of the SQS pulses with a pulse interval of 85.27 μs. (b) Single-pulse profile with a pulse width of 12.49 μs. (c) Spectrum of SQS pulses. (d) Output power vs pump power. The Q-switched threshold remains within 1 mW of the continuous-wave threshold. (e) Pulse width and repetition rate vs pump power. (f) Pulse energy and peak power vs pump power. (g) and (h) show tunable spectra of various SQS pulses with single and double peaks under different polarization states.

in the optical path difference, while the total transmission rate remains nearly constant. Figure 4(e) shows the amplified spontaneous emission spectrum before and after passing through the MZI, which is consistent with the calculations in Fig. 4(d).

C. Mechanism of self-Q-switching with interferometers

We propose two prerequisites for SQS generation based on experimental observations. First, there is an unpumped section in the EDF contributing to saturable absorption under low pumping conditions and further causing the bistability of continuous-wave and Q-switched operations. The physical mechanism can be elucidated using a three-level system without pumping, wherein the absorption rate correlates with the ground-state particle density. As the input intensity increases, the ground-state particle density decreases, leading to higher transmittance. This saturable absorption diminishes at high pump power when the EDF is fully pumped and saturated, explaining the absence of SQS at high powers. Another ion-pair interaction model is also used to interpret saturable absorption in EDF [36]. The second condition is the necessity of an MZI within the cavity. Based on the analysis and measurements of the MZI, it becomes evident that the MZI alone does not provide saturable absorption but a tunable filtering effect. While the MZI does not possess saturable absorption, it introduces random losses into the cavity with jitter of the optical path difference, which has no contribution to saturable absorption but plays a crucial role in exciting Q-switching by exciting the continuous-wave and Q-switching bistability into stable Q-switching as shown in Fig. 5. Given that spectral filtering may play a key role, the simulation cannot be restricted to a time-domain analysis. We developed a numerical model that takes into account both particle- and wavelike behaviors of a laser, enabling the description of Q-switching from the frequency domain (see Methods), and investigated the role of interferometers in SQS.

Figure 5 demonstrates the principles underlying the formation of SQS through simulation according to experimental configurations [37], where neither filtering fluctuations nor EDF saturation absorption can individually induce SQS while their combination enables the laser cavity to reach a Q-switched steady state. Figures 5(a)–5(c) illustrate the intracavity energy, gain dynamics, and spectral evolution when the unpumped section of EDF provides saturable absorption without MZI-induced fluctuations [38]. Figure 5(a) shows

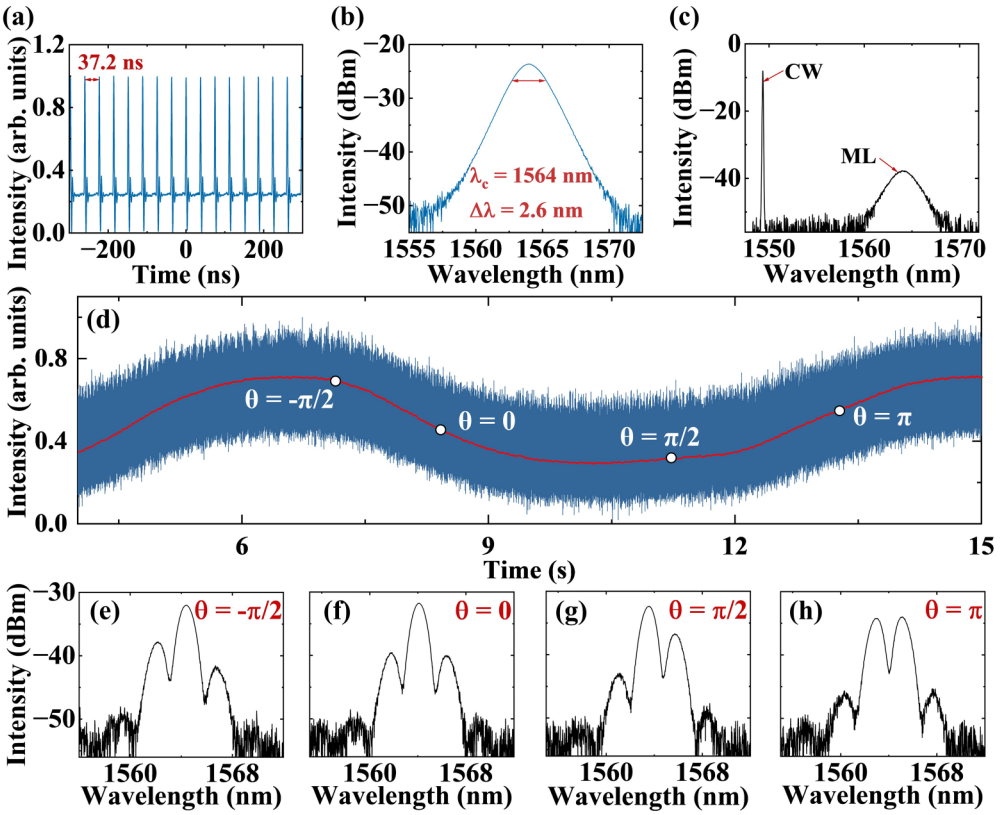

FIG. 3. Experimental measurements of the MZI. (a) and (b) Oscilloscope traces and spectrum of the mode-locked signal for measuring the MZI. (c) Spectrum of the complete test signal including mode-locked and continuous-wave components. (d) Oscilloscope trace of the test signal after MZI, with the red line representing the variation in continuous-wave intensity. The four points marked in the figure correspond to the phases in (e)–(h) of the bound-state-like structure.

the temporal evolution of the intracavity energy and the gain coefficient representing the difference between inverted particles and ground-state particles. Despite the presence of saturable absorption of EDF within the cavity, it only leads to energy oscillations but ultimately converging to a stable value. Figure 5(b) represents this process in a phase plane, with the horizontal axis representing the gain coefficient and the vertical axis representing the intracavity energy. The phase coordinates gradually approach a stable point during operation, representing a stable continuous-wave state. Figure 5(c) illustrates the frequency-domain evolution, showing the appearance of stable continuous waves within the cavity. It should be noted that saturated absorption alone does not guarantee passive Q-switching in the laser cavity but imparts bistable characteristics to the laser cavity, namely, continuous-wave and Q-switched states. Under merely gain fiber saturation absorption, the laser readily enters the continuous-wave state, as observed in both experiment and simulation. Figures 5(d)–5(f) show the results when there are MZI-induced fluctuations without a saturable absorption of EDF. The MZI filter curve is obtained from the simulation results in Fig. 4, and the random fluctuations are based on the actual sampled time-domain fluctuations. Figure 5(d) demonstrates that the energy and gain fluctuations rapidly converge to a fixed value, but exhibit fluctuations due to random losses after convergence. Figures 5(e) and 5(f) illustrate this process in a phase plane and frequency domain. Figures 5(g)–5(i) depict the evolution within the cavity when EDF saturable absorption and MZI fluctuations jointly interact. Figure 5(g) shows that with the progression of operation, stable Q-switched pulses are formed within the cavity, and Fig. 5(h) plots that the phase plane enters periodic oscillation. Figure 5(i) demonstrates the frequency domain evolving into a Q-switching operation.

III. DISCUSSION AND CONCLUSION

According to the results presented above, the mechanism behind SQS can be explained as follows. The saturable absorption provided by EDF creates bistability within the laser cavity, allowing it to exist in both a stable continuous-wave state and an oscillating Q-switched state characterized by periodic variations in energy and gain. While both states can stably coexist, most initial conditions tend to converge to the continuous-wave state such as those in Figs. 5(a)–5(c). On the other hand, the introduction of the MZI filters the cavity with random fluctuations, preventing the cavity from maintaining a constant steady state. This can be understood as applying a random force in the negative y direction to the phase points on the phase plane, forcing the laser to seek oscillating states.

Based on this interpretation, the peculiarities of the SQS phenomenon observed in experiments are explained reasonably within our model. First, the disappearance of SQS in the absence of the MZI occurs because the cavity converges to continuous waves when there are no filtering fluctuations. The small threshold for Q-switching is also evidence of MZI

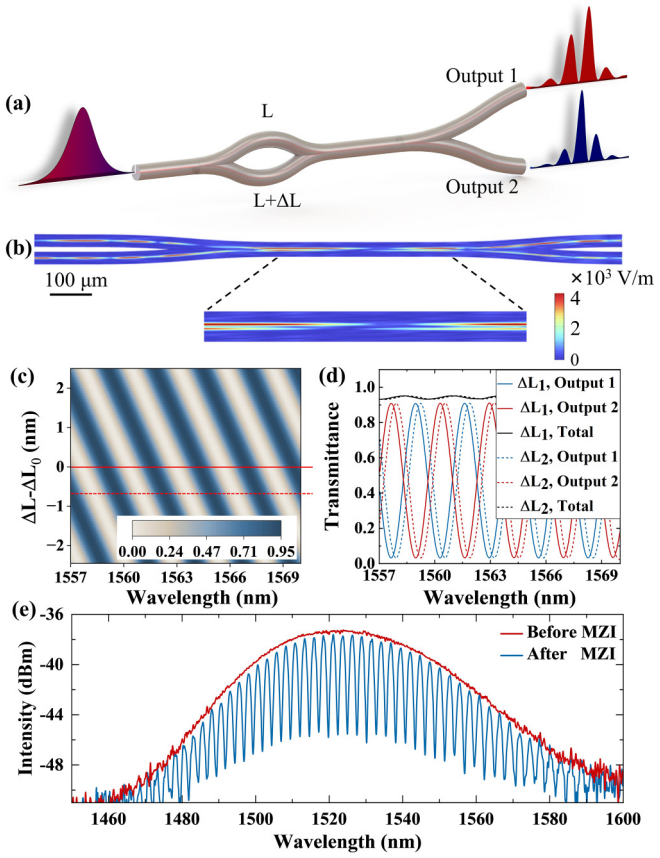

FIG. 4. Simulation of spectral filtering of MZI. (a) Schematic of the waveguide structure and filtering effect of the MZI, with an optical path difference set to 0.93 mm based on experimental measurements. (b) Distribution of the absolute value of electric field in the interferometric portion of the MZI after inputting a multifrequency continuous-wave laser. (c) Transmittance of the intracavity port of the MZI as a function of input wavelength and optical path difference. (d) Filter curves for the two output ports (red and blue) of the MZI at different optical path differences (solid and dashed lines), with the red curve corresponding to the red profile in (c). (e) Amplified spontaneous emission (ASE) spectra measured before and after passing through MZI.

fluctuations, which forces the laser to seek oscillating states regardless of intracavity power. Second, the wide polarization range for Q-switching to occur is because SQS does not depend on the polarization state, while the influence of the polarization state on the spectrum is through the change of the optical path difference and the associated filtering effect. The disappearance of Q-switching at high pump power is because the EDF is fully excited to the linear part of transmittance, causing the saturable absorption to vanish and the cavity no longer exhibits bistability. Even with MZI excitation, only weak fluctuations occur near the convergence point. Finally, the appearance of a complex multiwavelength operation is due to the fact that the MZI's external output is filtered in the opposite direction to the MZI within the cavity, causing the central wavelength to be filtered out, resulting in complex multiwavelength output. In summary, the existence of SQS depends on the MZI's filtering fluctuation, which stimulates the laser cavity to reach oscillating Q-switched states.

Apart from the MZI, other types of interferometers, such as Michelson interferometers, can also produce very similar SQS phenomena in the laser, as there is no fundamental difference in principle.

Compared to other explanations for SQS, our explanation reveals more experimental details, and the theoretical explanation involves the gain and absorption in EDF as well as jointly solving the time and spectral domains, which aligns well with the experimental results. However, it is important to note that this does not imply that our explanation is the only reasonable one for SQS. Although the MZI played a crucial role in our experiments and is relatively common in SQS within ring lasers, some studies have demonstrated SQS without the interferometers. While our theory can explain those cases as initial conditions falling within the range that can excite oscillating Q-switching states, other factors may also contribute to SQS.

In conclusion, we have revealed a SQS phenomenon based on interferometers and proposed a theory of SQS without relying on specific saturable absorbers. Numerical simulations have demonstrated the crucial role of the interferometer in SQS formation, which is also applicable in other types of lasers. This work reveals the principle of SQS with interferometers and offers critical insights into the excitation of SQS.

IV. METHODS

The simulation of self-Q-switching is based on a combination of a modified nonlinear Schrödinger equation and rate equation,

$$i\frac{\partial A}{\partial z} = \frac{\beta_2}{2}\frac{\partial^2 A}{\partial T^2} - \gamma|A^2|A + i\frac{1}{2}\frac{g_0}{1+E_{\text{pulse}}/E_{\text{sat}}}\left(1+T_2^2\frac{\partial^2}{\partial T^2}\right)A, \quad (1)$$

$$\frac{\partial g}{\partial t} = \frac{g_0 - g}{\tau_g} - \frac{g|A^2|}{E_{\text{sat}}}, \quad (2)$$

$$\alpha(I) = \alpha_{ns} + \frac{\alpha_0}{1+I/I_{\text{sat}}}, \quad (3)$$

where A is the slowly varying envelope, z is the propagation distance, $T = t - z/v_g$ is the reduced time in group velocity, β_2 is the group-velocity-dispersion parameter, T_2 is the dipole relaxation time, γ is the nonlinear coefficient, g is the gain coefficient, g_0 is the small signal gain coefficient, τ_g is the population relaxation time of dopants, E_{sat} is the saturation energy, α_{ns} is the linear loss, α_0 is the nonlinear loss, and I_{sat} is the saturation intensity. It should be noted that E_{sat} and I_{sat} describe gain saturation and saturable absorption processes respectively in this work. Equation (1) describes the nonlinear Schrödinger equation commonly used to depict laser propagation in optical fibers. The β_2, γ, and g terms represent dispersion, nonlinear, and gain terms, respectively. It is imperative to emphasize that the neglect of the nonlinear term has been undertaken ($\gamma = 0$), primarily due to the fact that the intracavity intensity remains insufficient to induce nonlinear effects. Furthermore, this deliberate omission eliminates the possibility of nonlinear effects contributing to the development of self-Q-switching. Equation (2) outlines the rate equation governing the dynamic evolution of gain

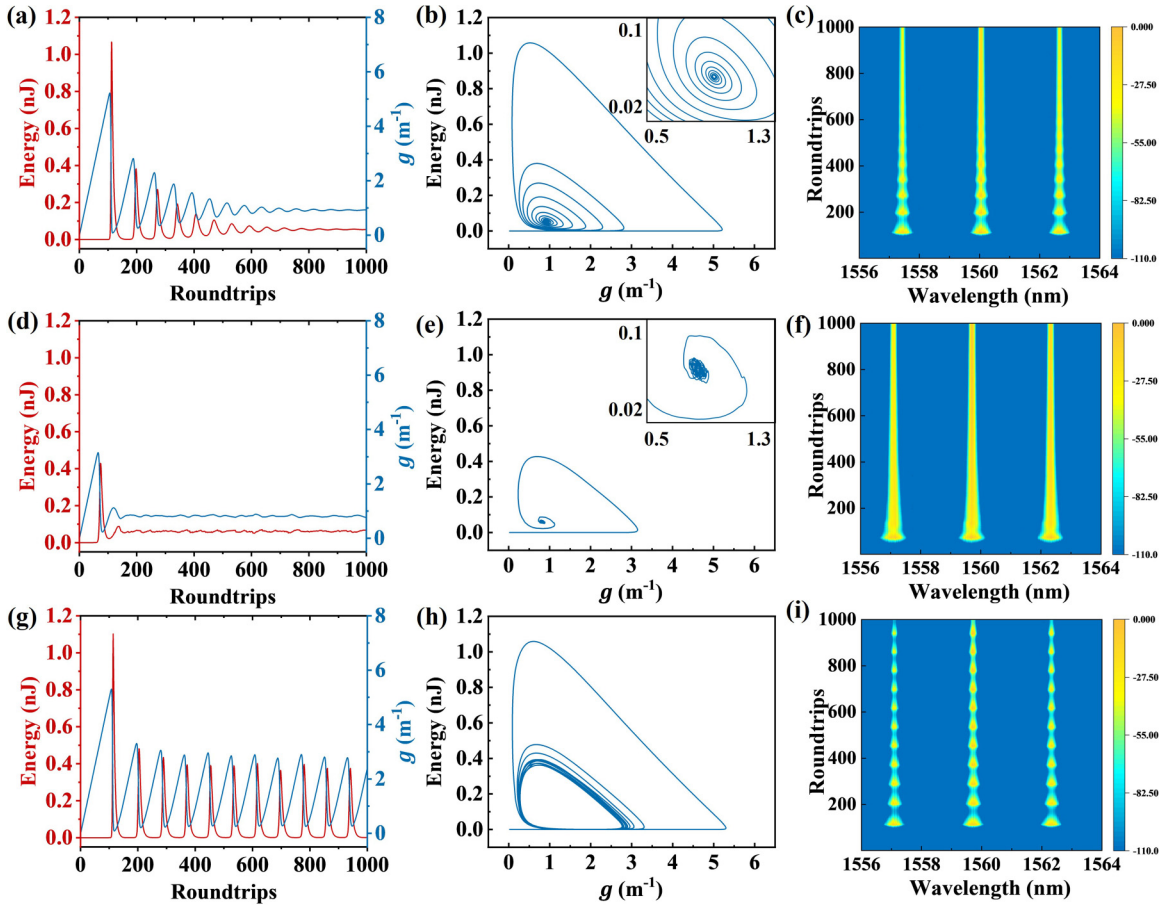

FIG. 5. Numerical simulation of SQS pulses based on interferometers. (a)–(c), (d)–(f), and (g)–(i) represent the temporal and frequency-domain evolution within the laser cavity when only the saturable absorption of EDF, only MZI filtering fluctuations, and both are present, respectively. The first column of composite figures demonstrates the evolution of intracavity energy and gain coefficients g, while the second column shows the phase plane of the two. The third column depicts the spectra evolution within the laser cavity. It is evident that in (a) and (d), the cavity energy converges to a constant value after oscillations, forming a continuous wave, which is also apparent in the frequency-domain evolution shown in (c) and (f). The oscillation process in (b) exhibits some differences, with a steeper phase curve, indicating a more intense conversion of gain into cavity energy, due to the presence of saturable absorption. The inset graph shows the enlarged view near the convergence point, exhibiting regular monotonicity. (e) shows residual oscillations even after convergence, resulting from filtering jitter. The inset shows irregular fluctuations near the convergence point. When both MZI and the saturable absorption of EDF are present, (g) and (i) illustrate Q-switching behavior in the time and frequency domains, while (h) demonstrates periodic cycling in the phase plane.

coefficient g including saturable gain of the pumped section of EDF, while Eq. (3) describes the saturable absorption from the unpumped section of the gain fiber. Based on the lumped model, Eq. (3) is calculated separately during laser evolution as $A_{\text{out}}(t) = A_{\text{in}}(t)\sqrt{1-\alpha}$. The model for the MZI is described as a filter curve correlated with the optical path difference, as illustrated in Figs. 4(c) and 4(d). This filter curve acts on the frequency-domain counterpart $\tilde{A}(\omega)$ of $A(T)$ in Eq. (1).

The parameters employed in our simulation align closely with experimental values. Specifically, the group-velocity dispersion parameters for both passive fibers and the gain fiber have been set to -22 and 12 ps^2/km, respectively. Meanwhile, key parameters such as the population relaxation time of dopants, the gain coefficient, and the saturation energy of the erbium-doped fiber are established at 10 ms, 37 dB, and 1 μJ, respectively. The initial intracavity condition is characterized by a 1-pW white-noise component. Additionally, because of the nonlinear absorption of erbium-doped fiber, the linear loss, nonlinear loss, and saturation intensity for the unpumped section of the erbium-doped fiber are configured at 0, 0.5, and 1 mW, respectively.

ACKNOWLEDGMENTS

This work was supported by the National Natural Science Foundation of China (Grant No. 62071016), the State Key Laboratory of Advanced Optical Communication Systems Networks, and College Students' Innovative Entrepreneurial Training Plan Program.

[1] M. Eichhorn and M. Pollnau, in *CLEO: Applications and Technology* (Optica Publishing Group, Washington, DC, 2012), pp. JW2A–29.

[2] Y. Wang and C.-Q. Xu, Prog. Quantum Electron. **31**, 131 (2007).

[3] F. Sauvage, V. P. Nguyen, Y. Li, A. Harizaj, J. Sebag, D. Roels, V. Van Havere, K. Peynshaert, R. Xiong, J. C. Fraire *et al.*, Nat. Nanotechnol. **17**, 552 (2022).

[4] J. M. Grevelink, D. Duke, R. L. van Leeuwen, E. Gonzalez, S. D. DeCoste, and R. R. Anderson, J. Am. Acad. Dermatol. **34**, 653 (1996).

[5] B. Kaifler, C. Geach, H. C. Büdenbender, A. Mezger, and M. Rapp, Nat. Commun. **13**, 6042 (2022).

[6] F. J. Fortes, J. Moros, P. Lucena, L. M. Cabalín, and J. J. Laserna, Anal. Chem. **85**, 640 (2013).

[7] L. Li, X. Yang, L. Zhou, W. Xie, Y. Wang, Y. Shen, Y. Yang, W. Yang, W. Wang, Z. Lv *et al.*, Photon. Res. **6**, 614 (2018).

[8] J. Beller and L. Shao, Light: Sci. Appl. **11**, 240 (2022).

[9] X. Liu, P. Tan, X. Ma, D. Wang, X. Jin, Y. Liu, B. Xu, L. Qiao, C. Qiu, B. Wang *et al.*, Science **376**, 371 (2022).

[10] X. Zhao, H. Jin, J. Liu, J. Chao, T. Liu, H. Zhang, G. Wang, W. Lyu, S. Wageh, O. A. Al-Hartomy *et al.*, Laser Photon. Rev. **16**, 2200386 (2022).

[11] S. Zhang, F. Lu, and J. Wang, Opt. Commun. **263**, 47 (2006).

[12] Z. Jia, C. Yao, Z. Kang, G. Qin, Y. Ohishi, and W.-P. Qin, J. Appl. Phys. **115**, 223103 (2014).

[13] A. V. Kir'yanov, Y. O. Barmenkov, M. Martinez-Gamez, and N. N. Il'ichev, Proc. SPIE **5622**, 373 (2004).

[14] T.-Y. Tsai and Y.-C. Fang, Opt. Express **17**, 21628 (2009).

[15] A. Kir'Yanov and Y. O. Barmenkov, Laser Phys. Lett. **3**, 498 (2006).

[16] S. C. Vicente, M. M. Gamez, A. V. Kir'yanov, Y. O. Barmenkov, and M. Andres, Quantum Electron. **34**, 310 (2004).

[17] R. Álvarez-Tamayo, M. Durán-Sánchez, O. Pottiez, B. Ibarra-Escamilla, M. Bello-Jiménez, and E. Kuzin, Laser Phys. **25**, 075102 (2015).

[18] Y. Chen, D. Lu, S. Ma, Z. Hu, J. Wang, and J. Wang, Results Opt. **7**, 100227 (2022).

[19] B. Zhang, L. Li, C. He, F. Tian, X. Yang, J. Cui, J. Zhang, and W. Sun, Opt. Laser Technol. **100**, 103 (2018).

[20] L. Wang, H. Huang, D. Shen, J. Zhang, H. Chen, and D. Tang, Laser Phys. Lett. **14**, 045803 (2017).

[21] J. Dong, A. Shirakawa, S. Huang, Y. Feng, K. Takaichi, M. Musha, K.-i. Ueda, and A. Kaminskii, Laser Phys. Lett. **2**, 387 (2005).

[22] J. Dong and K.-i. Ueda, Appl. Phys. Lett. **87**, 151102 (2005).

[23] P. K. Gupta, A. Singh, S. K. Sharma, P. K. Mukhopadhyay, K. S. Bindra, and S. M. Oak, Rev. Sci. Instrum. **83**, 046110 (2012).

[24] F. Sanchez, P. Le Boudec, P.-L. François, and G. Stephan, Phys. Rev. A **48**, 2220 (1993).

[25] A. Kir'yanov, N. Il'Ichev, and Y. O. Barmenkov, Laser Phys. Lett. **1**, 194 (2004).

[26] N. Doran and D. Wood, Opt. Lett. **13**, 56 (1988).

[27] L. Gui, X. Xiao, and C. Yang, J. Opt. Soc. Am. B **30**, 158 (2013).

[28] D. Y. Tang, W. S. Man, H. Y. Tam, and P. D. Drummond, Phys. Rev. A **64**, 033814 (2001).

[29] M. Z. Zulkifli, F. D. Muhammad, M. M. Azri, M. M. Yusof, K. Hamdan, S. A. Samsudin, and M. Yasin, Results Phys. **16**, 102949 (2020).

[30] W. Zhang, G. Wang, F. Xing, Z. Man, F. Zhang, K. Han, H. Zhang, and S. Fu, Opt. Express **28**, 14729 (2020).

[31] V. Matsas, T. Newson, D. Richardson, and D. N. Payne, Electron. Lett. **28**, 1391 (1992).

[32] D. Jachpure and R. Vijaya, Opt. Quantum Electron. **55**, 113 (2023).

[33] Y. I. Jhon, J. Koo, B. Anasori, M. Seo, J. H. Lee, Y. Gogotsi, and Y. M. Jhon, Adv. Mater. **29**, 1702496 (2017).

[34] Z. Luo, Y. Huang, J. Weng, H. Cheng, Z. Lin, B. Xu, Z. Cai, and H. Xu, Opt. Express **21**, 29516 (2013).

[35] Z. Sun, D. Popa, T. Hasan, F. Torrisi, F. Wang, E. J. Kelleher, J. C. Travers, V. Nicolosi, and A. C. Ferrari, Nano Res. **3**, 653 (2010).

[36] S. Colin, E. Contesse, P. Le Boudec, G. Stephan, and F. Sanchez, Opt. Lett. **21**, 1987 (1996).

[37] G. P. Agrawal, IEEE Photon. Technol. Lett. **2**, 875 (1990).

[38] D. Jachpure and R. Vijaya, J. Opt. **24**, 024007 (2022).